Nanoscale Research Letters

NANO EXPRESS Open Access

# Current Rectification in a Structure: $ReSe_2$/Au Contacts on Both Sides of $ReSe_2$

Tingting Miao[1†], Dongwei Yu[2†], Lei Xing[3†], Dawei Li[1], Liying Jiao[3], Weigang Ma[2*] and Xing Zhang[2]

## Abstract

Schottky effect of two-dimensional materials is important for nanoscale electrics. A $ReSe_2$ flake is transferred to be suspended between an Au sink and an Au nanofilm. This device is initially designed to measure the transport properties of the $ReSe_2$ flake. However, a rectification behavior is observed in the experiment from 273 to 340 K. The rectification coefficient is about 10. The microstructure and elements composition are systematically analyzed. The $ReSe_2$ flake and the Au film are found to be in contact with the Si substrate from the scanning electron microscope image in slant view of 45°. The $ReSe_2$/Si and Si/Au contacts are p-n heterojunction and Schottky contacts. Asymmetry of both contacts results in the rectification behavior. The prediction based on the thermionic emission theory agrees well with experimental data.

**Keywords:** $ReSe_2$, Rectification, Two-dimensional materials

## Introduction

Rectification behaviors of metal-semiconductor contacts, where the current varies with the direction of the applied voltage, are widely used in Schottky barrier diode, field effect transistor (FET), and metal-oxide-semiconductor FET. Schottky explained the behavior by depletion layers on the semiconductor side of such interfaces [1]. Differences of electron work function between metal and semiconductor lead to the rectification behavior named Schottky effect [2]. The contact between metal and two-dimensional (2D) semiconductor materials is a Schottky contact when the metal has a higher electron work function than an n-type 2D semiconductor materials or lower electron work function than a p-type 2D semiconductor. The Schottky effect of metal/2D materials has great applications in micro-photo detectors, micro-FETs, gas sensors, and phototransistors [3]. Among 2D materials, transition metal dichalcogenides (TMDs) have attracted much attention because they have a sizable bandgap [3] and the bandgap transits from indirect to direct as the thickness is reduced to monolayer [4]. The bandgap ensures that TMDs can be used for many applications, i.e., FETs and solar cells [3]. TMDs can be also used in thermoelectric field [5], which has drawn wide attention [6–9]. Many experiments have been done to explore properties and applications of TMDs such as $MoS_2$, $MoSe_2$, $WSe_2$, and $WS_2$. Lopez-Sanchez et al. [10] made ultrasensitive monolayer phototransistors with $MoS_2$. Britnell et al. [11] made a $WS_2$/graphene heterostructure and demonstrated its application in photovoltaic device. $WSe_2$, as an ambipolar semiconductor, was controlled with double electrostatic gates to fabricate a light-emitting diode [12, 13]. Among TMDs, $ReSe_2$ is different from other group VI TMDs because $ReSe_2$ belongs to group VII TMDs with an extra electron in *d* orbitals, which leads to strong in-plane anisotropy [14]. A few studies have explored the electrical properties of $ReSe_2$ due to its special band structure. Current rectification is explored with a $ReSe_2$/$WS_2$ p-n heterojunction [15] and $ReSe_2$/$MoS_2$ p-n heterojunction [16]. FET is made to investigate the electrical properties of metal/semiconductor contacts like $ReSe_2$/metal or $ReS_2$/metal [17–19].

In this letter, a $ReSe_2$ flake is suspended across an Au sink and an Au nanoribbon electrode. The device is originally designed to measure the thermal and electrical conductivities of the $ReSe_2$ flake. Measurements were performed at 340 K, 310 K, 280 K, and 273 K.

* Correspondence: maweigang@tsinghua.edu.cn
†Tingting Miao, Dongwei Yu and Lei Xing contributed equally to this work.
[2]Key Laboratory for Thermal Science and Power Engineering of Ministry of Education, Department of Engineering Mechanics, Tsinghua University, Beijing 100084, China
Full list of author information is available at the end of the article

## Methods

Firstly, the Si substrate with Au electrodes was fabricated. The 400-μm-thick undoped Si substrate was oxidized to form a 180-nm-thick $SiO_2$ layer after initial cleaning, and a 320-nm-thick electron beam resist was deposited on the $SiO_2$ surface by means of spin coating. Au was deposited by physical vapor deposition to fabricate the Au nano-electrodes and the Au nanofilm in the pattern which was prepared by electron beam lithography. By putting the sample into the photoresist developer, the electron beam resist was etched and the Au electrode and film were left. At last, the $SiO_2$ layer is etched by buffered hydrofluoric acid and the Si layer under the Au nanofilm is etched by $CF_4$ plasma to fabricate a suspended nanofilm which is about 6 μm above the Si substrate.

$ReSe_2$ flakes were synthesized by chemical-vapor-transition on a copper substrate. A $ReSe_2$ flake was transferred to the Au electrodes to fabricate Au-$ReSe_2$-Au contacts using the wetting transfer method, in which the $ReSe_2$ nanoribbon with the copper substrate was coated by polymethylmethacrylate (PMMA) and floated onto the etching solution to etch the copper substrate. After the copper substrate was peeled off, the PPMA-coated $ReSe_2$ flake was accurately moved above the Si substrate with Au nano-electrodes by the fixed-point transfer platform. Then, the PMMA was cut by laser and the PMMA-coated $ReSe_2$ flake landed to be suspended between the Au nanofilm and the Au nano-electrode. Finally, the PMMA was removed by dipping the sample into a potassium hydroxide solution bath for 3 h. The scanning electron microscope (SEM) image of the fabricated Au electrode-$ReSe_2$ flake-Au nanoribbon (Au-$ReSe_2$-Au) junctions in vertical view to the substrate is shown in Fig. 1a. The $ReSe_2$ flake was in contact with an Au nanoribbon in section B and in contact with Au electrode in section C. Figure 1b shows the schematic diagram of the device.

The direction along A-B-C is defined as positive, or vice versa, and a direct current was applied. The voltage, *V*, across the Au-$ReSe_2$-Au junctions was measured by a high accuracy digital multimeter (Keitheley 2002, 8.5 digits), while the current, *I*, was determined through measuring the voltage across a reference resistor in series. The *I-V* curves of the $ReSe_2$/Au junctions for forward and inverse voltage were measured at different temperatures in a physical property measurement system (quantum design).

## Results and Discussion

Figure 2 shows the measured *I-V* curves at 273 K, 280 K, 310 K, and 340 K. Significant asymmetries in the *I-V* curves are observed at all the measured temperatures, indicating unusual rectifying behavior. Currents at 277

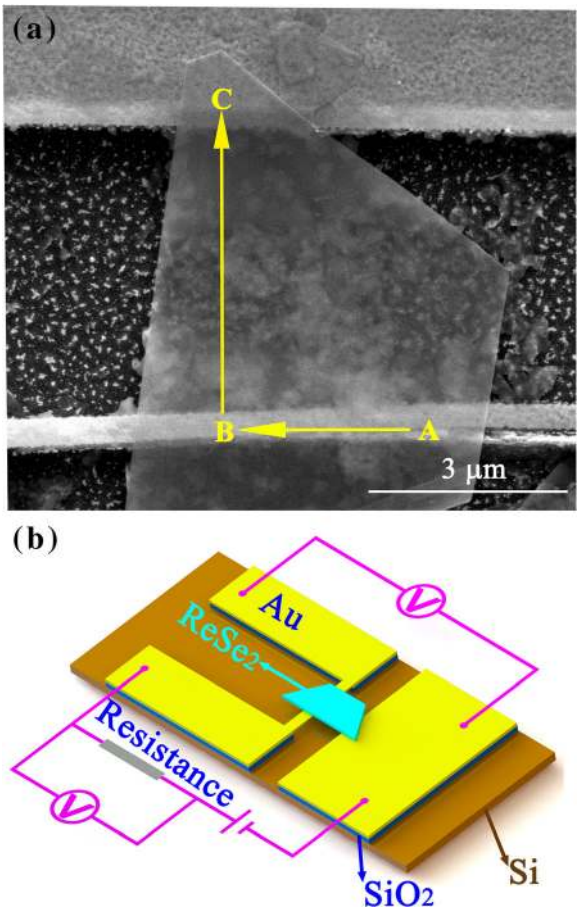


**Fig. 1** **a** SEM image of the device in vertical view to the substrate and the positive current direction and **b** schematic diagram of the measurement device

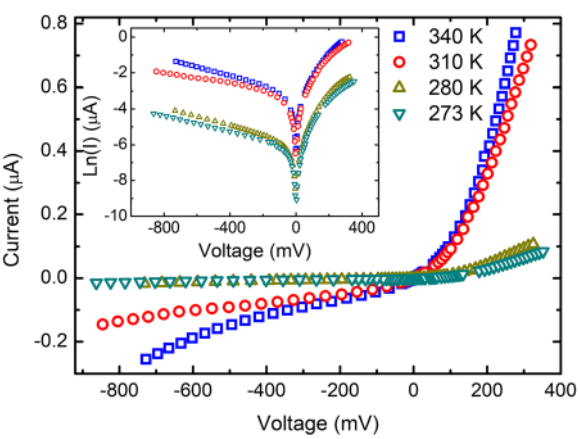


**Fig. 2** Current-voltage characteristics of Au-ReSe2-Au junctions at 273 K, 280 K, 310 K, and 340 K

mV and − 277 mV are used to calculate the current rectification ratio at each temperature, and the rectifying ratio is about 10. The current increases with the temperature for a given voltage.

To explore the mechanism responsible for the unusual rectification, the microstructure of the $ReSe_2$ flake was detected by an atomic force microscope [(AFM), Cypher, Oxford Instruments] and a Raman spectrometer (Jovin Yvon T64000, excitation wavelength 532 nm). The AFM image of the $ReSe_2$ flake is shown in Fig. 3a–c, and the determined average thickness is 28 nm based on the cross-sectional height profile along the white line. The Raman spectrum consisting of up to 13 expected lines with high signal strength is shown in Fig. 3d, corresponding well with the spectrum detected by Wolverson et al. [4] and revealing the triclinic crystal structure of the present $ReSe_2$ flake.

Figure 4 is the SEM image of the $ReSe_2$ flake in slant view of 45° showing that the $ReSe_2$ flake and the Au nanofilm are in contact with the Si substrate. $ReSe_2$-Au contact has been shown the Ohmic contact in previous study [20] which is not responsible for the rectification behavior in this experiment. The circuit is constituted of the Au-$ReSe_2$-Au and the Au-$ReSe_2$-Si-Au junctions. Figure 5 shows the schematic of the circuit. The Si-Au contact has been shown the Schottky contact [21].

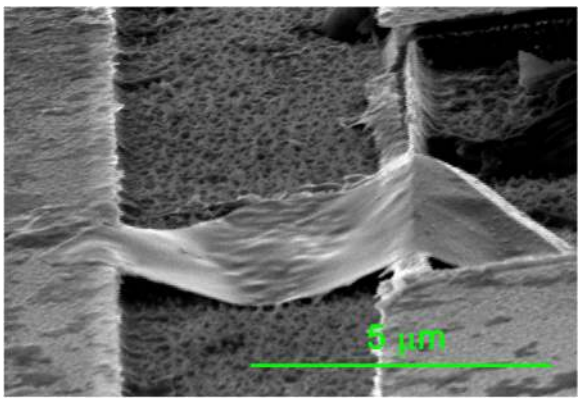


**Fig. 4** SEM image of the $ReSe_2$ flake and the Au nanofilm in slant view of 45°

Figure 6 shows the energy dispersive spectroscopy (EDS) data. The map sum spectrum of $ReSe_2$ is acquired in section 1 and 2. The average chemical formula is $ReSe_{1.67}$ which has a higher ratio of Re than $ReSe_2$ and gives the $ReSe_2$ flake p-type semiconductor properties. Therefore, the $ReSe_2$-Si contact is a p-n heterojunction and exhibits the rectification behavior. Asymmetry of both rectification contacts results in the rectification behavior.

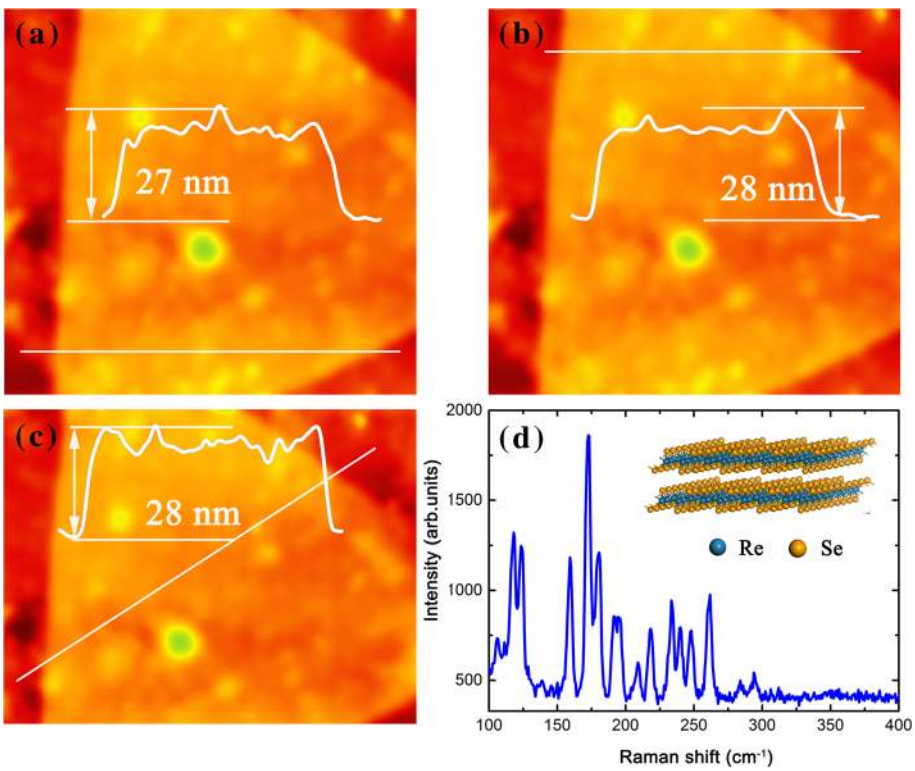


**Fig. 3** **a**, **b**, and **c** AFM image and thickness of ReSe2, and **d** Raman spectrum and crystal structure of ReSe2

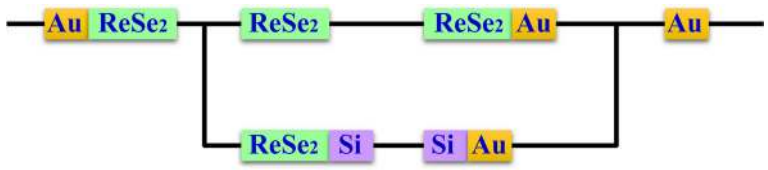


**Fig. 5** Schematic of the circuit

The current can be determined by the following equation in both the Schottky contact and the p-n heterojunction [22, 23]:

$$I = I_0 e^{qV/nkT}\left(1-e^{-qV/kT}\right) \tag{1}$$

$$I_0 = AA^* T^2 e^{-q\Phi_B/kT} \tag{2}$$

where $I_0$ is the saturation current, $q$ is the electronic charge, $k$ is the Boltzmann constant, $V$ is voltage applied across the junction, $A$ is the contact area, $A^*$ is the effective Richardson constant, $\Phi_B$ is the apparent barrier height, and $T$ is the measurement temperature. The temperature-dependent ideality factor $n$ represents the level that the contact departs from an ideal Schottky contact.

A calculation based on Eq. (1) is made to examine the analysis for the rectification behavior. Currents of the $ReSe_2$-Si contact, $I_1$, and the Si-Au contact, $I_2$, are expressed by:

$$I_1 = I_{01} e^{qV/n_1 kT}\left(1-e^{-qV/kT}\right), \tag{3}$$

$$I_2 = I_{02} e^{-qV/n_2 kT}\left(e^{qV/kT}-1\right). \tag{4}$$

Figure 7 shows that the numerical results agree well with experimental data. The numerical parameters are shown in Table 1. The reverse saturation current of the $ReSe_2$-Si contact is larger than the Si-Au contact because the contact area of the $ReSe_2$-Si contact is much larger as shown in Fig. 4. The reverse saturation current of both contacts increase with temperature, indicating that the electrical conductivities of both contacts exhibit rectification behavior as shown in Eq. (2).

The ideality factor of the $ReSe_2$-Si contact is larger than the Si-Au contact due to different contact conditions and crystal structures. Figure 4 shows that the surface of the Si substrate is rough due to the etching solution, which makes the $ReSe_2$-Si contact inhomogeneous. The inhomogeneous contact leads to the large ideality factor [24, 25]. The rough surface also produces a large number of trapping states which results in a large ideality factor [26]. Additionally, different contact types make different ideality factors. The $ReSe_2$-Si contact is the p-n heterojunction, and the $ReSe_2$ and Si have different crystal structures, triclinic for $ReSe_2$ and faced-centered cubic for Si. The lattice mismatch always leads to edge dislocation [27] and produces high density of trap states [26], making the $ReSe_2$-Si contact deviate from the ideal contact and have a large ideality factor

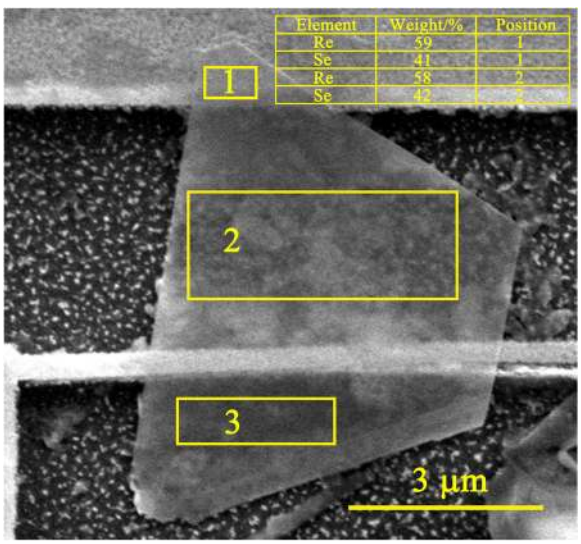


**Fig. 6** EDS data of $ReSe_2$ is on the top right corner of the image. Boxes 1 and 2 represent two measured sections

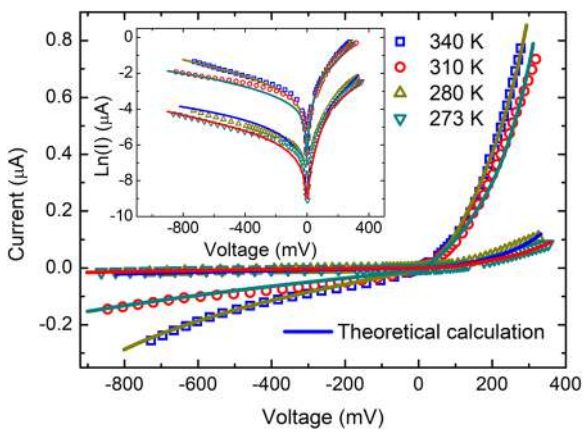


**Fig. 7** Comparison of *I-V* curves of the experimental results and the calculated

**Table 1** Calculated ideality factor for $ReSe_2$-Si and Si-Au contacts

| Temperature/K | $I_{01}$/μA | $I_{02}$/μA | $n_1$ | $n_2$ |
|---|---|---|---|---|
| 273 | 0.0095 | 0.0002 | 1.43 | 1.10 |
| 280 | 0.014 | 0.0003 | 1.46 | 1.08 |
| 310 | 0.084 | 0.011 | 1.46 | 1.06 |
| 340 | 0.170 | 0.010 | 1.46 | 1.11 |

[27]. The Si-Au is the metal semiconductor contact, and the crystal structure of Si has few effects on the ideality factor. The ideality factors of both contacts change little with temperature. It can be explained by Eq. (5) as reported by Khurelbaatar et al. [28],

$$n = \frac{q}{kT}\frac{dV}{d\ \ln I}. \tag{5}$$

Equation (5) shows that the ideality factor is inversely proportional to the temperature. The ideality factor significantly decreases with temperature only at low temperature and changes slowly when the temperature is over 300 K [28, 29]. However, as shown in Table 1, the reverse saturation current increases significantly with the temperature which is different from the ideality factor. It can be explained by Eq. (2). According to Eq. (2), the reverse saturation current increases with temperature because $T^2$ and exp $(-q\Phi_B/kT)$ increase with temperature. Due to the exponential relationship between exp $(-q\Phi_B/kT)$ and $-q\Phi_B/kT$, exp $(-q\Phi_B/kT)$ increases significantly with temperature. Based on the research by Zhu et al [30], $q\Phi_B$ of the Au/Si contact in the experiment at 273 K and 295 K are 0.77 eV and 0.79 eV, respectively. The calculated results show that the reverse saturation current at 295 K is six times as much as the reverse saturation current at 273 K, explaining why the reverse saturation current increases significantly with temperature.

## Conclusions

In conclusion, a rectification behavior is observed in the contacts where a $ReSe_2$ flake suspended across Au substrate and Au nanofilm at different temperature. The SEM image of the suspended $ReSe_2$ flake in slant view of 45° shows that the $ReSe_2$ flake and the Au nanofilm are in contact with the Si substrate and the EDS map illustrated the elements composition, $ReSe_{1.67}$. The contact between the $ReSe_2$ flake and the Si substrate is responsible for the rectification behavior. The $ReSe_2$-Si and Si-Au contacts are both rectification contacts forming another circuit, and asymmetry of both contacts results in the apparent rectification behavior. The calculated results based on Schottky current equation considered the Si-Au Schottky contact, and the $ReSe_2$-Si p-n heterojunction agrees well with experiments results.

### Abbreviations

2D: Two-dimensional; AFM: Atomic force microscope; EDS: Energy dispersive spectroscopy; FET: Field effect transistor; PMMA: Polymethylmethacrylate; SEM: Scanning electron microscope; TMD: Transition metal dichalcogenides

### Acknowledgements

Not applicable

### Funding

This work was supported by the National Natural Science Foundation of China (Grant Nos. 51776224, 51576105, 51636002, 51827807, and 51336009), the Science Fund for Creative Research Groups (Grant No. 51621062), Beijing Municipal Science & Technology Commission (No Z161100002116030), and the Tsinghua University Initiative Scientific Research Program.

### Availability of Data and Materials

All data are fully available without restriction.

### Authors' Contributions

All authors contributed to the preparation of the manuscript and to the discussion. All authors read and approved the final manuscript.

### Competing Interests

The authors declare that they have no competing interests.

## Publisher's Note



### Author details

[1]Beijing Key Laboratory of Process Fluid Filtration and Separation, College of Mechanical and Transportation Engineering, China University of Petroleum-Beijing, Beijing 102249, China. [2]Key Laboratory for Thermal Science and Power Engineering of Ministry of Education, Department of Engineering Mechanics, Tsinghua University, Beijing 100084, China. [3]Department of Chemistry, Tsinghua University, Beijing 100084, China.

Received: 24 October 2018 Accepted: 20 December 2018
Published online: 03 January 2019

### References

1. Schmitsdorf RF, Kampen TU, Monch W (1997) Explanation of the linear correlation between barrier heights and ideality factors of real metal-semiconductor contacts by laterally nonuniform Schottky barriers. J Vac Sci Technol B 15(4):1221–1226.
2. Rhoderick EH (1982) Metal-semiconductor contacts. IEE Proc I Commun Speech Vis 129(1):1–14.
3. Cho AJ, Namgung SD, Kim H, Kwon JY (2017) Electric and photovoltaic characteristics of a multi-layer $ReS_2$/$ReSe_2$ heterostructure. APL Materials 5: 076101.
4. Wolverson D, Crampin S, Kazemi AS, Ilie A, Bending SJ (2014) Raman spectra of monolayer, few-layer, and bulk $ReSe_2$: an anisotropic layered semiconductor. ACS Nano 8(11):11154–11164.
5. Zhang G, Zhang YW (2017) Thermoelectric properties of two-dimensional transition metal dichalcogenides. J Mater Chem C 5:7684–7698.
6. Pan T, Gong T, Yang W, Wu Y (2018) Numerical study on the thermal stress and its formation mechanism of a thermoelectric device. J Therm Sci 27(3): 249–258.
7. Zhou ZG, Zhu DS, Wu HX, Zhang HS (2013) Modeling, experimental study on the heat transfer characteristics of thermoelectric generator. J Therm Sci 22(1):48–54.
8. Morita SI, Tanimura K, Hayamizu Y, Yamada T, Horibe A, Haruki N (2016) Study of cycle output improvement by work-fluid including phase change material. J Therm Sci 25(6):558–563.
9. Qi X, Ma W, Zhang X, Zhang C (2018) Raman characterization and transport properties of morphology-dependent two-dimensional $Bi_2Te_3$ nanofilms. Appl Surf Sci 457:41–48.
10. Lopez-sanchez O, Lembke D, Kayci M, Radenovic A, Kis A (2013) Ultrasensitive photodetectors based on monolayer $MoS_2$. Nat Nanotechnol 8(7):497–501.

11. Britnell L, Ribeiro RM, Eckmann A, Jalil R, Belle BD, Mishchenko A (2013) Strong light-matter interactions in heterostructures of atomically thin films. Science 340(6138):1311–1314.
12. Ross JS, Klement P, Jones AM, Ghimire NJ, Yan J, Mandrus DG (2014) Electrically tunable excitonic light-emitting diodes based on monolayer $WSe_2$ p–n junctions. Nat Nanotechnol 9(4):268–272.
13. Baugher BWH, Churchill HOH, Yang Y, Jarillo-Herrero P (2014) Optoelectronic devices based on electrically tunable p–n diodes in a monolayer dichalcogenide. Nat Nanotechnol 9:262–267.
14. Yang S, Wang C, Sahin H, Chen H, Li Y, Li SS, Suslu A, Peeters FM, Liu Q, Li J, Tongay S (2015) Tuning the optical, magnetic, and electrical properties of $ReSe_2$ by nanoscale strain engineering. Nano Lett 15(3):1660–1666.
15. Wang C, Yang S, Xiong W, Xia C, Cai H, Chen B, Wang X, Zhang X, Wei Z, Tongay S, Li J, Liu Q (2016) Gate-tunable diode-like current rectification and ambipolar transport in multilayer van der Waals $ReSe_2/WS_2$ p-n heterojunctions. Phys Chem Chem Phys 18(40):27750–27753.
16. Wang X, Huang L, Peng Y, Huo N, Wu K, Xia C, Wei Z, Tongay S, Li J (2016) Enhanced rectification, transport property and photocurrent generation of multilayer $ReSe_2/MoS_2$ p-n heterojunctions. Nano Res 9(2):507–516.
17. Corbett CM, McClellan C, Rai A, Sonde SS, Tutuc E, Banerjee SK (2015) Field effect transistors with current saturation and voltage gain in ultrathin $ReS_2$. ACS Nano 9(1):363–370.
18. Corbet CM, Sonde SS, Tutuc E, Banerjee SK (2016) Improved contact resistance in $ReSe_2$ thin film field-effect transistors. Appl Phys Lett 108: 162104.
19. Park JY, Joe HE, Yoon HS, Yoo S, Kim T, Kang K, Min BK, Jun SC (2017) Contact effect of $ReS_2$/metal interface. ACS Appl Mater Interfaces 9(31): 26325–26332.
20. Yang S, Tongay S, Li Y, Yue Q, Xia JB, Li SS, Li J, Wei SH (2014) Layer-dependent electrical and optoelectronic responses of $ReSe_2$ nanosheet transistors. Nanoscale 6(13):7226–7231.
21. Balsano R, Matsubayashi A, LaBella VP (2013) Schottky barrier height measurements of Cu/Si(001), Ag/Si(001), and Au/Si(001) interfaces utilizing ballistic electron emission microscopy and ballistic hole emission microscopy. AIP Adv 3:112110.
22. Kang WP, Davidson JL, Gurbuz Y, Kerns DV (1995) Temperature-dependence and effect of series resistance on the electrical characteristics of a polycrystalline diamond metal-insulator-semiconductor diode. J Appl Phys 78(2):1101–1107.
23. Ito H (1986) Generation-recombination current in the emitter-base junction of AlGaAs/GaAs HBTs. Jpn J Appl Phys 25(9):1400–1404.
24. Tung RT (1991) Electron-transport of inhomogeneous Schottky barriers. Appl Phys Lett 58(24):2821–2823.
25. Sullivan JP, Tung RT, Pinto MR, Graham WR (1991) Electron-transport of inhomogeneous Schottky barriers - a numerical study. J Appl Phys 70(12): 7403–7424.
26. Gokarna A, Pavaskar NR, Sathaye SD, Ganesan V, Bhoraskar SV (2002) Electroluminescence from heterojunctions of nanocrystalline CdS and ZnS with porous silicon. J Appl Phys 92(4):2118–2124.
27. Majumdar S, Banerji P (2009) Temperature dependent electrical transport in p-ZnO/n-Si heterojunction formed by pulsed laser deposition. J Appl Phys 105:043704.
28. Khurelbaatar Z, Kil YH, Shim KH, Cho H, Kim MJ, Kim YT, Choi CJ (2015) Temperature dependent current transport mechanism in graphene/germanium Schottky barrier diode. J Semicond Technol Sci 15(1):7–15.
29. Lee TC, Chen TP, Au HL, Fung S, Beling CD (1993) The effect of the temperature-dependence of the ideality factor on metal-semiconductor solar devices. Semicond Sci Technol 8(7):1357–1360.
30. Cardon F, Blondeel A, Clauws P, Ru GP, Zhu S, Detavernier C (2001) Electrical characterization of Ar-ion-bombardment-induced damage in Au/Si and PtSi/Si Schottky barrier contacts. Semicond Sci Technol 16(2):83–90.